European Journal of Human Genetics (2020) 28:64–75
https://doi.org/10.1038/s41431-019-0374-9

ARTICLE

DPH1 syndrome: two novel variants and structural and functional analyses of seven missense variants identified in syndromic patients

Roser Urreizti[1] · Klaus Mayer[2] · Gilad D. Evrony[3] · Edith Said[4,5] · Laura Castilla-Vallmanya[1] · Neal A. L. Cody[6,7] · Guillem Plasencia[8] · Bruce D. Gelb[6,9,10] · Daniel Grinberg[1] · Ulrich Brinkmann[2] · Bryn D. Webb[6,9,10] · Susanna Balcells[1]

Received: 23 October 2018 / Revised: 21 February 2019 / Accepted: 1 March 2019 / Published online: 15 March 2019

Abstract

DPH1 variants have been associated with an ultra-rare and severe neurodevelopmental disorder, mainly characterized by variable developmental delay, short stature, dysmorphic features, and sparse hair. We have identified four new patients (from two different families) carrying novel variants in *DPH1*, enriching the clinical delineation of the DPH1 syndrome. Using a diphtheria toxin ADP-ribosylation assay, we have analyzed the activity of seven identified variants and demonstrated compromised function for five of them [p.(Leu234Pro); p.(Ala411Argfs*91); p.(Leu164Pro); p.(Leu125Pro); and p.(Tyr112Cys)]. We have built a homology model of the human DPH1–DPH2 heterodimer and have performed molecular dynamics simulations to study the effect of these variants on the catalytic sites as well as on the interactions between subunits of the heterodimer. The results show correlation between loss of activity, reduced size of the opening to the catalytic site, and changes in the size of the catalytic site with clinical severity. This is the first report of functional tests of *DPH1* variants associated with the DPH1 syndrome. We demonstrate that the in vitro assay for DPH1 protein activity, together with structural modeling, are useful tools for assessing the effect of the variants on DPH1 function and may be used for predicting patient outcomes and prognoses.

Introduction

Diphthamide is a unique post-translationally modified histidine residue found only in eukaryotic and archaeal translation elongation factor 2 (EF2). Diphthamide is conserved across all eukaryotes, and notably, is the target of diphtheria toxin (DT). DT catalyzes the transfer of ADP-ribose from nicotinamide adenine dinucleotide (NAD^+) to diphthamide, thereby inhibiting protein synthesis and leading to cell death [1].

These authors contributed equally: Roser Urreizti, Klaus Mayer, Gilad D. Evrony

These authors contributed equally: Ulrich Brinkmann, Bryn D. Webb, Susanna Balcells

Supplementary information The online version of this article (https://doi.org/10.1038/s41431-019-0374-9) contains supplementary material, which is available to authorized users.

✉ Roser Urreizti
roseruf@yahoo.es

1 Department of Genetics, Microbiology and Statistics, Faculty of Biology, University of Barcelona, IBUB, IRSJD, CIBERER, Barcelona, Spain

2 Roche Pharma Research and Early Development. Large Molecule Research, Roche Innovation Center, Munich, Nonnenwald 2, 82377 Penzberg, Germany

3 Center for Human Genetics & Genomics, New York University Langone Health, New York, NY, USA

4 Section of Medical Genetics, Mater dei Hospital, Msida, Malta

5 Department of Anatomy and Cell Biology, University of Malta, Msida, Malta

6 Department of Genetics and Genomic Sciences, Icahn School of Medicine at Mount Sinai, New York, NY, USA

7 Sema4, Stamford, CT, USA

8 Lead Molecular Design, S.L, Sant Cugat del Vallés, Spain

9 Mindich Child Health and Development Institute, Icahn School of Medicine at Mount Sinai, New York, NY, USA

10 Department of Pediatrics, Icahn School of Medicine at Mount Sinai, New York, NY, USA

Table 1 Clinical features observed in patients with *DPH1* mutations

Reference	Alazami et al. [4]	Loucks et al. [5]	Riazuddin et al. [6]	Sekiguchi et al. [8]	Nakajima et al. [7]	Present study	Present study	Total (%)
Geographical origin	Saudi Arabia	North America	Pakistan	Iran	Japan	Malta	Yemen	
Mutation (at protein level)	p.(Leu234Pro)	p.(Met6Lys)	p.(Pro382Ser)	p.(Ala411Argfs*91)	p.(Glu97Lysfs*8)/ p.(Leu164Pro)	p.(Leu125Pro)	p.(Tyr112Cys)	
Mutation (at cDNA level)	c.701T>C	c.17T>A	c.1144C>T	c.1227delG	c.289delG/c.491T>C	c.374T>C	c.335A>G	
rs SNP ID	rs730882250	rs749267261	rs765677788	–	–	rs200530055	rs772969956	
Allele count (freq.) in gnomAD	1 (0.000004)	1 (0.000004)	4 (0.00001)	–	–	79 (0.00028)	2 (0.000008)	
In vitro enzyme activity	Reduced	as wt	as wt	Reduced	Reduced (for p.Leu164Pro)	Reduced	Reduced	
Number of patients	4	4	2	2	1	2	2	17
Developmental delay/intellectual disability	4/4	4/4	2/2[(3)]	2/2	1/1	2/2	2/2	17/17 (100)
CNS malformations	4/4	0/2	NA	2/2	1/1	1/1	1/1	9/11 (81.8)
Hypotonia	4/4	0/4	1/2	0/2	0/1	2/2	2/2	9/17 (52.9)
Epilepsy	NA	1/1	NA	1/2	0/1	2/2	1/2	5/8 (62.5)
Short stature	4/4	3/4	NA	2/2	1/1	2/2	2/2	14/15 (93.3)
Abnormal head circumference	NA	macroc. 1/4	NA	NA	microc.	microc.	Relative macroc.	6/9 (66.7)
Unusual skull shape	4/4	4/4	NA	2/2	1/1	2/2	2/2	15/15 (100)
Craniofacial dysmorphic features	4/4	4/4	2/2	2/2	1/1	2/2	2/2	17/17 (100)
Dental abnormalities	NA	1/4	NA	2/2	NA	2/2	2/2	7/10 (70)
Sparse hair on scalp, eye lashes, or eyebrows	4/4	4/4	NA	2/2	1/1	2/2	2/2	15/15 (100)
Hand/foot anomalies	4/4 [(2)]	2/2	NA	2/2 [(4)]	NA	2/2	2/2	12/12 (100)
Abnormal toe nails	NA	3/4	NA	NA	NA	2/2	1/2	6/8 (75)

Table 1 (continued)

Reference	Alazami et al. [4]	Loucks et al. [5]	Riazuddin et al. [6]	Sekiguchi et al. [8]	Nakajima et al. [7]	Present study	Present study	Total (%)
Heart malformation/ abnormality [(1)]	3/4	0/4	NA	1/2	0/1	1/2	2/2	7/15 (46.7)
Renal disease	3/4	1/4	NA	0/2	0/1	NA	0/2	4/13 (30.8)
Genitalia anomalies	2/4	NA	NA	NA	1/1	1/2	1/2	5/9 (55.6)
Early lethality	3/4	0/4	0/2	0/2 [(5)]	0/1	1/2	0/2	4/17 (23.5)
Other features (in all the patients if not specified otherwise)	Bifid uvula, hypotonia	Visual impairment (2/4), sleep apnea (1/4), bilateral inguinal hernia (1/4), ADHD (1/4), anxiety (1/4), failure to thrive (1/4)	Autism, motor weakness	Cleft palate, widely spaced teeth, scleral pigmentation, bilateral single transverse palmar crease, kyphoscoliosis (1/2), ADHD and anxiety (1/2)	Bilateral single transverse palmer creases, IUGR, required mechanical ventilation at birth	Bilateral hernia (1/2), keratoconus, hypothyroidism (1/2)	Anxiety (1/2); unilateral single transverse palmar crease (1/2)	

CNS Central nervous System, *NA* Not assessed or no information available, *macroc* macrocephaly, *microc* microcephaly, *ADHD* attention-deficit hyperactivity disorder, *IGUR* intrauterine growth restriction. (1) Ventricular septal defect, dilated cardiomyopathy, aortic stenosis, atrial septal defect, tetralogy of Fallot… (2) camptodactyly; (3) mild. Both patients with autism; (4) flat foot; (5) an older brother died at 6 month of sudden infant death but the *DPH1* mutation has not been assessed

DPH1 (diphtamide biosynthesis 1, OMIM *603527) encodes the enzyme [2-(3-amino-3-carboxypropyl) histidine synthase subunit 1; EC 2.5.1.108], which is required for the first step in the synthesis of diphthamide and, therefore, is essential for generating the diphthamide modification of eukaryotic EF2 (eEF2). *DPH1* is also a tumor-suppressor gene with a crucial role in the regulation of cell proliferation, embryonic development, and tumorigenesis [2, 3].

Recently, autosomal recessive variants in *DPH1* have been associated with a rare neurodevelopmental disorder, known as DEDSSH (Developmental delay with short stature, dysmorphic features, and sparse hair; MIM #616901), with clinical features, including intellectual disability, short stature, and craniofacial and ectodermal anomalies. So far, five independent groups of DEDSSH patients have been published: one family with four affected members of Saudi Arabian origin [4], a group of four patients from three consanguineous families from an American genetic isolate [5], a Pakistani family with two affected patients [6], a Japanese patient [7], and two siblings from a consanguineous Iranian family [8]. All but one of the DPH1 variants identified in these patients were missense (Table 1).

Because the functionality of DPH1 directly affects diphthamide synthesis and consequently the ADP-ribosylation (ADPR) by DT of eEF2's diphthamide residue [9], ADPR assays can be used to probe the presence or absence of diphthamide and thereby indirectly test the functionality of DPH1 [10]. Here, using whole-exome sequencing (WES), we have identified two novel homozygous missense variants in *DPH1* in two unrelated families with DEDSSH. We applied the ADPR assay to functionally validate and confirm the pathogenicity of these variants as well as all DPH1 variants previously published. Next, we built a homology model of the DPH1–DPH2 heterodimer to elucidate possible mechanisms by which the variants disrupt protein function. Finally, we established genotype–phenotype correlations for this rare disease, which we propose to rename as DPH1 syndrome.

Results

Clinical report

Family 1

Patient 1 The patient is a 31-year-old man born in the USA, who was initially clinically diagnosed with Opitz C syndrome. He is the first son of a Maltese couple and was born at 38 weeks gestation by vaginal delivery with a birth weight of 2.35 Kg (−2.5 SD Z-score). He suffered from neonatal seizures and was nursed in the neonatal unit for

2 months because of feeding difficulties and multiple congenital anomalies. He had a high and broad forehead with pronounced metopic suture and trigonocephaly and an open posterior fontanelle. There were capillary hemangiomata on the face, his ears were reportedly low-set and protruding, and the palate was highly arched. Also noted were short digits and clinodactyly of the 5th fingers. He was congenitally hypotonic and did not sit until 17 months. Severe psychomotor delay and failure to thrive were noted from early childhood. He also required treatment for hypothyroidism. As an infant, he developed keratoconus. Orchidopexy and bilateral inguinal hernia repair were performed at 1 year of age. Other anomalies included two fused vertebrae, bony defects of hands and feet, and a horseshoe-shaped kidney. A brain MRI performed when he was 11-year-old showed dilated ventricles and cavum septi pellucidi.

During development, his growth curves for weight and height were below the fifth centile and he suffered from repeated respiratory infections, none of which required hospitalization. He has been tube-fed throughout most of his life. At 18 years of age, he had an episode of congestive heart failure and his echocardiogram showed dilated cardiomyopathy.

On examination at 21 years of age, the patient was severely developmentally delayed, non-ambulatory, with no speech and no sphincter control. He was hypotonic with cortical spasticity. He had short stature (−8.4 SD Z-score), low weight (−13.6 SD Z-score), and low BMI (−2.8 SD Z-score). He was severely microcephalic with an occipital frontal circumference (OFC) of 46.1 cm (−6.1 SD Z-score). The shape of the skull was trigonocephalic with prominent metopic and sagittal sutures, sparse hair and soft left side of the posterior end of the sagittal suture with no hair and temporal prominence. He had a high, broad, triangular forehead with bitemporal prominence and supraorbital ridges. The face was characterized by marked ocular telecanthus (inner canthal distance 3.5 cm; interpupillary distance 7 cm, outer canthal distance 11 cm), bilateral epicanthic folds, downslanting palpebral fissures, keratoconus, ocular proptosis, short nose with depressed nasal bridge, and a small mouth that could not be fully opened. He had a short neck, broad thorax with increased internipple distance, venous reticulum, abnormal fat distribution in trunk and no axillary hair. The hands were small with short tapered fingers. He had loose skin on the back, right hand with a single transverse palmar crease, and cutaneous syndactyly at second, third, and fourth ray. The feet were described to have hallux valgus with hypoplastic, overriding toes. He had a micropenis, hypoplastic scrotum, undescended testes, and a lack of pubic hair. The patient also presented with webbing at the knees and neurological muscle wasting in lower limbs.

Patient 2 She was the younger sister of Patient 1 and died at the age of 20 years after a hospitalization for a severe respiratory tract infection. She was born by elective caesarian section for breech presentation. Apgar scores were 2 and 9, at 1 and 5 min, respectively. At birth, dysmorphic facial features similar to her brother were noted, and it was evident that she had the same syndrome. CT-scan showed leukomalacia, cavum septum pellucidum, ventricular dilatation, synostosis of metopic suture, agenesis of the corpus callosum, and leukodystrophy. Her EEG was abnormal, with very frequent runs of slow generalized spikes and slow wave discharge. At 7 years of age, her bone age was advanced (9 years).

When examined at 10 years of age, she had profound intellectual disability and growth delay, was wheelchair-bound, and had no sphincter control. She presented with microcephaly (OFC −6.2 SD Z-score), short stature (105 cm; −5 SD Z-score), and low BMD (−5 SD Z-score) with a weight of 12 kg (−7.6 SD Z-score). The dysmorphic features were more marked than her brother's. She presented with trigonocephaly and dolichocephaly with prominent sagittal suture, proptosis, downslanting palpebral fissures, telecanthus, a small nose and mouth. Her ears were prominent with low-set auricles, simpler than her brother's. She also had pectus excavatum, venous reticulum, hypoplasia of the nipples, increased inter-nipple distance, and fat in the breast areas. Her hands and feet were similar to her brother's and her knee joints were hyperextensible. She had normal genitalia. Neurologically, she had central hypotonia with brisk tendon reflexes and clonus of the feet.

Family 2

Patient 3 The patient is a 20-month-old male of Yemeni (Bedouin) ancestry born to healthy parents who are first cousins. Prenatal history was notable for a diagnosis of tetralogy of Fallot made by fetal echocardiogram at 20 weeks of gestation. The patient was born at 38 weeks gestation by vaginal delivery with a birth weight of 2.99 kg (−0.94 SD Z-score), length of 41.5 cm (−3.12 SD Z-score), and head circumference of 34 cm (−0.89 SD Z-score). Dysmorphic features were noted at birth, including frontal bossing, epicanthal folds, a depressed nasal bridge, and a short nose with an upturned nasal tip. Echocardiogram performed after delivery confirmed tetralogy of Fallot and a closed patent ductus arteriosus. Renal sonogram was normal. Surgical repair of tetralogy of Fallot was performed at 4 months of age. vEEG completed at 4 months of age due to decreased responsiveness after surgery was notable for diffuse cerebral dysfunction, but no seizure activity. Head CT was significant for mild diffuse generalized cerebral and cerebellar volume loss. At 5 months of age, the patient

received a G-tube due to poor feeding. Head ultrasound at 6 months revealed moderate pan-ventricular dilatation. His MRI completed at 6 months revealed diffuse prominence of the ventricular system and extra-axial fluid spaces, likely secondary to underlying parenchymal volume loss (Supplementary Figure 1). At 17 months of age, the patient presented with fever and a fixed right eye gaze deviation lasting ~30 min, suggesting a febrile seizure. An EEG completed shortly after this event was negative. He was recently diagnosed with obstructive sleep apnea.

On examination at 20 months of age, head circumference was at the 0.65 SD Z-score, weight was at −0.787 SD Z-score, and height was short at −2.4 SD Z-score. The patient appeared macrocephalic with prominent frontal bossing, broad forehead, and high anterior hairline. Sparse, thin, and coarse hair was noted along with sparse eyebrows and absent eye lashes. Eyes appeared hyperteloric with downslanting palpebral fissures and epicanthal folds. Ears had overfolded helices bilaterally and micrognathia was noted. He had small peg-shaped teeth, normal palmar creases, short tapered digits, and pes planus. Nails were normal. He had significant hypotonia and gross motor delay, but was able to sit unsupported and support weight on his legs when held. He had loose skin over his hands and feet.

Chromosome analysis was normal. Chromosomal microarray did not reveal any pathogenic CNVs, but was notable for 223 Mb of absence of heterozygosity (AOH) (~7.8% of autosomal genome), consistent with the history of consanguinity (Supplementary Table 1).

Patient 4 The patient is the 7-year-old brother of Patient 3. Prenatal history was unremarkable. The patient was born at 37 weeks gestation by normal spontaneous vaginal delivery. He required 2 days in the neonatal intensive care unit for respiratory support with supplemental oxygen. At 3 months of age, the patient was diagnosed with obstructive sleep apnea and required supplemental oxygen at night for several years. He had a hydrocele, which resolved by 1 year of age. An echocardiogram completed at 5 years of age was notable for a moderately dilated left ventricle with eccentric left ventricular hypertrophy. He has recently had multiple seizures, and EEG revealed suboptimal organization, mild generalized slowing, and occasional bilateral, independent hemispheric spikes. Developmental delays were noted from a young age.

On examination, at 7 years of age, head circumference was at 0.31 SD Z-score, weight was low at −2.8 SD Z-score, and short stature was present with height at −4.0SD Z-score. Dysmorphic features included frontal bossing, broad forehead, high anterior hairline, low-set and posteriorly rotated ears, short philtrum, and small, peg-shaped teeth. Sparse, thin, and coarse hair was noted with sparse eyebrows and absent eye lashes. His right hand had a single transverse palmar crease. He had tapered digits, pes planus, and dysplastic toe nails. He had a micropenis. He was nonverbal and had significant hypotonia and gross motor delay, but was able to sit unsupported.

Genetic investigations

Family 1

WES was performed on both affected sibs and parents (four individuals) and revealed six candidate variants in five genes (Supplementary Table 2). In particular, one homozygous variant was identified as "disease causing" in both affected siblings: *DPH1* c.374 T > C; p.(Leu125Pro) (NM_001383.4), inherited from both heterozygous parents. This variant has been submitted to the Leiden Open Variation Database (http://lovd.nl/3.0/). The remaining variants were classified as likely benign changes or variants of unknown significance (VUS).

Family 2

WES was performed for the proband and the father. Variants called by WES were filtered for call quality, low frequency in the population, and predicted deleteriousness, yielding 103 variants in 76 genes (Supplementary Table 3). An additional biological context filter identifying variants in genes known or predicted to cause "Tetralogy of Fallot" or "Developmental Delay" yielded a single variant: *DPH1* c.335 A > G; p.(Tyr112Cys). This variant was homozygous in the proband and heterozygous in the father. The variant was confirmed by Sanger sequencing in the proband and father. Additionally, Sanger sequencing confirmed that the older affected brother is also homozygous for this variant. This variant has been submitted to the Leiden Open Variation Database (http://lovd.nl/3.0/).

Protein alignments

In order to assess the conservation of the residues affected by the missense variants identified in our patients and those described in the literature (listed in Table 1), the DPH1 protein sequences from 80 different eukaryotic species were aligned for comparison. In general, the central part of the protein (positions 80 to 310 of the human DPH1) was highly conserved, while the N- and C-termini displayed less conservation. Human DPH1 Met6 corresponds to the initiation codon in most other mammals, while in bonobos (*Pan paniscus*), two sequences with different initiation codon are described (see Supplementary Figure 3). Tyr at position 112 is conserved among all the analyzed species up to and including fungi, while Leu125, Leu164, and Leu234 are conserved in nearly all of them. Finally, Pro382, at the

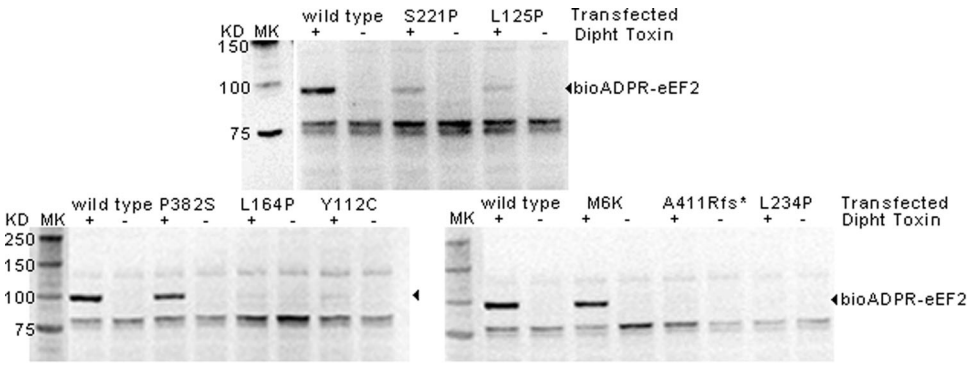

Fig. 1 Assay for diphthamide deficiency and DPH1 function in DPH1-knockout (DPH1ko) cells. Extracts of DPH1ko cells transfected with wild-type or mutant DPH1 variants were subjected to diphtheria toxin (DT)-mediated biotin–ADP-ribosylation of diphthamide. Assay activity was then detected by probing membrane blots with enzyme-conjugated streptavidin. eEF2 protein is sized 100 kDa. Extracts of DPH1ko cells expressing plasmid-encoded wild-type DPH1 were included as positive controls. Reactions with no DT served as specificity controls. Background bands are biotinylated cellular proteins that provide controls for equal loading of protein

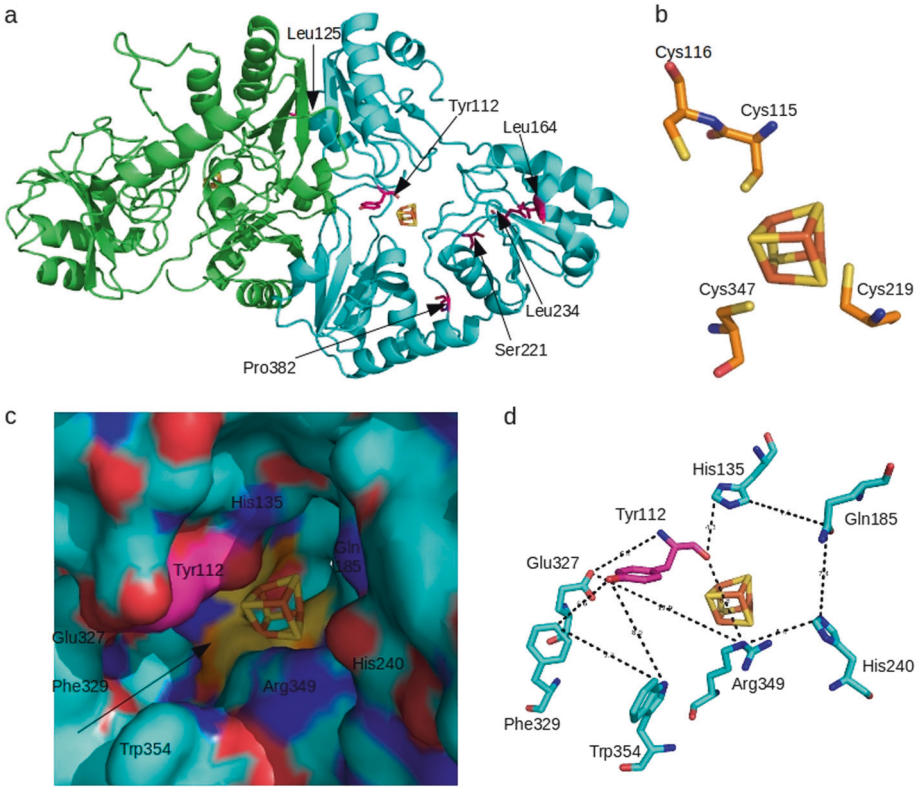

Fig. 2 Homology model of human DPH1–DPH2 heterodimer. Upper panels: **a** Human DPH1–DPH2 model, with DPH2 subunit on the left (in green) and DPH1 subunit on the right (in blue) with a cube-shaped [4Fe–4S] cluster to the right. Arrows show the positions of Tyr112, Leu125, Leu164, Ser221, Leu234, and Pro382. **b** DPH1 subunit Cys116, Cys115, Cys219, and Cys347 form a plane around the [4Fe–4S] cluster (its position in the figure, not optimized, is shown here for reference). Lower panels: **c** Potential iron–sulfur cluster entry points in DPH1 model. Gate A, shown with an arrow in the lower left side of the image, and gate B in the center of the image. **d** Residues forming gate A and gate B potential entry points

less conserved C-terminus of the protein, is present in all the analyzed mammals, *Xenopus*, most birds and insects.

Biochemical investigation of all DPH1 missense variants identified so far in the DPH1 syndrome

We applied an ADP-ribosylation (ADPR) assay to test the functional impact of all previously identified DPH1 missense variants. Diphtheria toxin catalyzes the transfer of ADP-ribose from NAD^+ to the diphthamide residue on eEF2. In this assay, biotinylated NAD is used, which can also function as a toxin substrate, such that in cell extracts exposed to DT and biotinylated NAD, biotin–ADP is transferred to diphthamide–eEF2. eEF2 without diphthamide does not become ADP-ribosylated, and hence, is not labeled with biotin.

The degree to which diphthamide is present on eEF2 can thereby be visualized. Figure 1 shows the results of these ADPR assays. Extracts of MCF7 cells with inactivated DPH1 genes (DPH1ko cells with both alleles inactivated [11]) were transfected with plasmids that encode either wild-type DPH1 or DPH1 variants. Those variants included

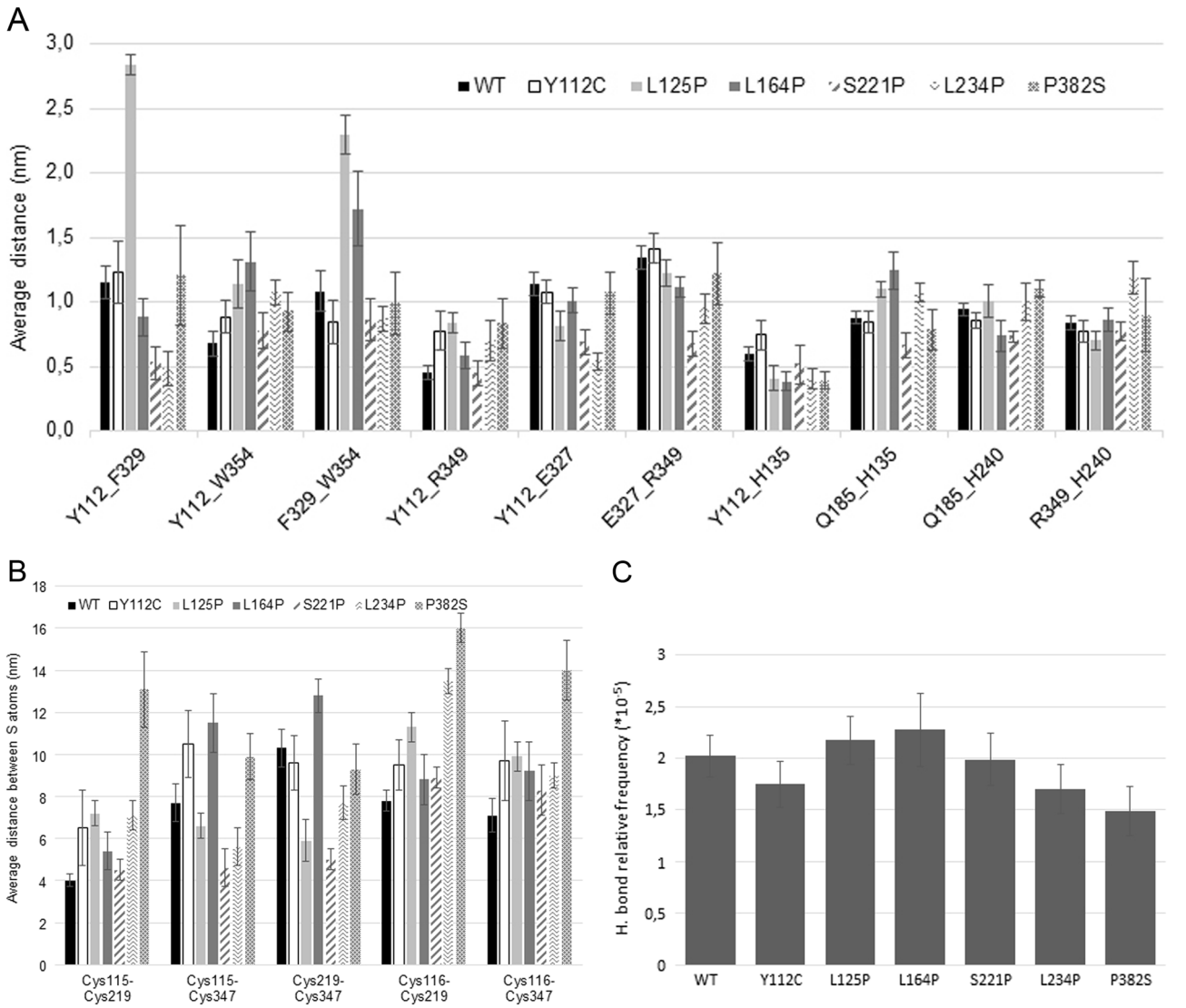

Fig. 3 Distance analysis of human DPH1 model binding site. **a** Average distance in nanometers between atoms that form potential entry points for the iron–sulfur cluster into DPH1 (error bars represent the standard deviation). **b** Average distance in nanometers (error bars show the standard deviation) between side chain sulfur atoms of cysteine residues potentially involved in binding iron–sulfur cluster in human DPH1. **c** Average relative number of hydrogen bonds between DPH1 and DPH2 (out of all possible hydrogen bonds) along each simulation, (error bars show the standard deviation)

a p.(Ser221Pro) variant that was originally present in the catalogue of somatic variants in cancer (as COSM 1381407, https://cancer.sanger.ac.uk/cosmic/) labeled as SNP. We have previously observed that this variant has reduced functionality [10] and have therefore applied it as a control in our assays. The other DPH1 variants that we applied to our assay are those that were identified in the patients described above (Table 1). Compared with cells transfected with wild-type DPH1, cells expressing the variants p.(Tyr112Cys), p.(Leu125Pro), p.(Leu164Pro), p.(Leu234-Pro), and p.(Ala411Argfs*91) contained reduced amounts of ADP-ribosylated eEF2. This reflects reduced presence of diphthamide on eEF2, and therefore reduced DPH1 functionality compared with wild-type DPH1. The reduction in functionality of these variants is similar to or even more pronounced than that observed for the previously tested p.(Ser221Pro) variant [10]. In contrast, no difference in ADP-ribosylation of eEF2 was observed for cells expressing the variants p.(Met6Lys) and p.(Pro382Ser), indicating that these variants do not significantly affect DPH1 function.

Homology models of *Homosapiens* DPH1–DPH2

Human DPH1–DPH2 heterodimers were modeled using the *Pyrococcus horikoshii* DPH2–DPH2 homodimer structure [12] (PDBID: 3LZD) as a template (Supplementary Figure 3). Our heterodimeric models contained wild-type DPH2 and either the wild-type DPH1, the p.(Ser221Pro)

variant previously described [10], or mutants identified in DPH1 syndrome patients, namely p.(Tyr112Cys), p.(Leu125Pro), p.(Leu164Pro), p.(Leu234Pro), or p.(Pro382Ser) (Fig. 2a). Leu125 is located in the DPH1–DPH2 interface, close to DPH2 residues Thr290, Gln295, Arg297, and Ala318, and we hypothesize that mutant p.(Leu125Pro) may affect the DPH1–DPH2 interaction. DPH1 residues Tyr112, Leu164, Ser221, Leu234, and Pro382 are located far from the DPH1–DPH2 interface, and we propose that the effect of the variants described at these residues is through structural changes that may interfere with functionality.

DPH1 belongs to a superfamily of enzymes that contain a cysteine-bound [4Fe–4S] cluster and can generate radicals of S-adenosylmethionine [13]. Two hybrid and coimmunoprecipitation experiments with yeast and mouse DPH1 suggest that it forms a catalytic complex with DPH2 [14], a highly homologous protein also containing a [4Fe–4S] cluster that forms homodimers. The crystal structure of the functional DPH2 homodimer of *Pyrococcus horikoshii*, an archaeal microorganism, shows each monomer bound to a [4Fe–4S] cluster through the sulfur atoms of three conserved cysteine residues separated by more than 100 residues [12]. The three cysteine residues involved in binding the [4Fe–4S] iron–sulfur cluster in *P. horikoshii* DPH2 homodimer, Cys59, Cys163, and Cys287, were aligned to Cys115, Cys219, and Cys347 residues of human DPH1 (Fig. 2b).

In mammals, the iron–sulfur cluster biogenesis is a complex multistep process, whereby the iron–sulfur cluster is synthesized and transferred to its recipient target [15]. In our models, DPH1 has only one suitable opening for the insertion of the iron–sulfur cluster into the cavity close to the conserved cysteine residues (Fig. 2c). This opening contains two regions, which we name gates A and B. Gate A is a table-shaped tunnel defined by five residues: Phe329 and Trp354 on the outer side, and Glu327 and Arg349 on the inner side, that form the four pillars, and Tyr112, located on top of these four residues. Gate B is a hole with boundaries defined by residues Tyr112, Arg349, His135, Gln185, and His240 (Fig. 2d). Thus, variant Tyr112Cys could hinder the insertion of the iron–sulfur cluster to its final destination.

A proposed reaction mechanism for these types of enzymes involves one iron atom of the cluster, whereas the remaining three iron atoms are bonded to three SH groups of cysteine residues [16]. In *Eukaryota* and *Archaea* organisms, these three cysteine residues are farther away in the sequence of DPH1 than in other members of the radical SAM superfamily, which display a characteristic CX3CX2C motif [13]. We propose that the DPH1 variants p.(Leu164Pro), p.(Ser221Pro), p.(Leu234Pro), and p.(Pro382Ser) might introduce conformational changes that separate Cys115, Cys219, and Cys347 and prevent or impair their binding to the iron–sulfur cluster.

Molecular dynamics simulations

To further investigate the effect of the studied variants on DPH1 structure, molecular dynamics simulations of human DPH1–DPH2 models containing variants p.(Tyr112Cys), p.(Leu125Pro), p.(Leu164Pro), p.(Ser221Pro), p.(Leu234-Pro), and p.(Pro382Ser) were compared with simulations of the wild-type DPH1–DPH2 model. The iron–sulfur cluster was removed from all the models prior to the simulation to allow unrestrained movement of cysteine residues putatively involved in its binding.

First, we measured if the variants reduced the dimensions of gates A and B (Fig. 3a). While no statistical analysis can be performed, large alterations can be observed for variants p.(Ser221Pro) and p.(Leu234Pro), showing a reduced distance between Tyr112 and Phe329, Tyr112 and Glu327, and between Glu327 and Arg349. p.(Ser221Pro) also showed a slightly reduced distance between gate B residues Gln185 and His135. All these results suggest that gate A could be smaller in p.(Leu234Pro) and p.(Ser221Pro) mutant proteins, and might impair the entry of the cube-shaped iron cluster, which has diagonal length of ~4 Å.

On the other hand, p.(Leu125Pro) showed increased distances for gate A residues (for Tyr112-Phe329 and Phe329–Trp354) and p.(Leu164Pro) showed an increased distance for Phe329–Trp354 residues. These increased distances could be hampering the retention of the iron–cluster at the catalytic site. The precise distances between residues are listed in Supplementary Table 4.

The crystallographic structure of *P. horikoshii* DPH2–DPH2 homodimer [12] and the proposed reaction mechanism [16] suggest that only three DPH1 cysteine residues (amongst 115, 116, 219, and 347) are covalently bound to the three iron atoms of the iron–sulfur cluster through their side chain sulfur. The distance between all possible pairs of S atoms of Cys115, Cys116, Cys219, and Cys347 was measured in simulations of *P. horikoshii* and human monomeric DPH1. The distances involving Cys115 were closer to the distances observed between *P. horikoshii* template cysteine residues (Cys59, Cys163, and Cys287) than those involving Cys116, suggesting that Cys115 is better located than Cys116 to bind the iron–sulfur cluster (Supplementary Table 4b).

Next, we analyzed the effect of the variants on the inter-cysteine distances on human DPH1–DPH2 heterodimeric complexes (Fig. 3b), which could hinder the binding of the iron–sulfur cluster in the catalytic site. Variants p.(Leu125Pro), p.(Ser221Pro), and p.(Leu234Pro) showed a reduction in Cys115–Cys347 and Cys219–Cys347 distances. On the other hand, p.(Leu234Pro) showed an

increased Cys116–Cys219 distance and p.(Pro382Ser) showed large distance increases for the Cys115–Cys219, Cys116–Cys219, and Cys116–Cys347 pairs.

To investigate the effect on the strength of DPH1–DPH2 interaction of these variants, the total number of hydrogen bonds between atoms of each subunit was measured in our simulations, relative to the total number of potential hydrogen bonds (Fig. 3c). Variant p.(Pro382Ser) showed the highest reduction in the number of hydrogen bonds between both subunits, whereas p.(Leu234Pro) and p.(Tyr112Cys) showed a slight decrease and all other variants including p.(Leu125Pro), located on the interphase between DPH1 and DPH2, were similar to the wild-type.

In general, all five missense variants analyzed by molecular dynamics simulations displayed some structural alteration compared with the wild-type or affected a residue located in a critical position for the iron–sulfur cluster insertion.

Discussion

To date, a total of 16 patients have been published with homozygous or compound heterozygous variants in *DPH1*, including the ones presented here [4–8]. An emerging DPH1 syndrome phenotype is being delineated, which is characterized mainly by variable developmental delay or intellectual disability, unusual skull shape with or without craniosynostosis (most often with a broad forehead), sparse hair, and a variety of dysmorphic features (Table 1). Most patients also have short stature. Central nervous system malformations are present in nearly all the assessed patients with the exception of two cases [5]. Also, a variety of cardiac defects have been observed in 7 out of 15 of the assessed patients [4, 8], including one of the patients in Family 1 and two patients in Family 2 described here. Abnormal toe nails, observed in Family 1 and one of the affected siblings in Family 2, have also been described for three of the four North American patients [5]. Hypotonia observed in both of siblings of Family 1 has also been previously reported in the patients bearing the p.(Leu234Pro) variant [4]. Moreover, motor weakness is mentioned in one of the two patients with the p.(Pro382Ser) variant [6]. Surprisingly, both micro- and macrocephaly have been observed previously [5, 7]. In addition, abnormal genitalia, micropenis (as observed in one sibling in Family 2), and hypospadias (as observed in the male patient of Family 1), have been previously reported [4, 7].

In order to better understand the effect of each variant and to try to establish genotype–phenotype correlations, we assayed the function of each of the previously described missense variants, together with the variants identified in the patients presented here and the frameshift p.(Ala411Argfs*91) variant that is allegedly not affected by the NMD degradation process, since it generates a stop codon in the last exon further downstream from the wild-type stop codon. This is the first time in which *DPH1* variants associated with the DPH1 syndrome have been functionally and bioinformatically assessed. Generally, the DPH1 activity measured for each variant by our assay correlated with the severity of the corresponding patients' clinical presentation.

In the four cases bearing the p.(Met6Lys) variant, the intellectual disability was often referred to as mild or moderate [5], with no mention to the heart or CNS malformations. Interestingly, in our assay, the p.(Met6Lys) variant as well as the p.(Pro382Ser) variant, showed similar activity compared with wild-type DPH1. The protein alignment shows that Met6 is the translation initiation codon in a majority of species, including primates. In humans, Met6 could be acting as an alternative initiation codon and its loss could reduce overall DPH1 protein levels in vivo, which may not be reflected in our functional assay that uses an exogenous expression construct. In this sense, as stated in Uniprot [17] (Q9BZG8; accessed June 2018), it is uncertain whether Met1 or Met6 is the initiator. A variety of bioinformatic tools predict both Met1 and Met6 as putative initiation codons, with Met1 having the highest scores [18, 19]. Together, these data support the pathogenicity of the p.(Met6Lys) variant and its association with a milder presentation, and future characterization of it could be conducted by analyzing the amount of DPH1 protein in the p.(Met6Lys) homozygous patients' fibroblasts. The clinical information regarding the patients bearing the p.(Pro382Ser) is scarce, but the mention of autism in one patient and "good learner" in the other (while intellectual disability is mentioned for both), and the absence of any reference to CNS or heart conditions, suggests a milder phenotype. This variant retains its activity in vitro at levels comparable with wild-type, but as mentioned above, small in vitro activity reductions may not be detectable in this system. Our in silico models suggest that p.(Pro382Ser) decreases the interaction between DPH1 and DPH2 and increases the distances between the cysteine residues involved in binding the iron–sulfur cluster, which might be causing mild alterations in the protein functionality, not reflected in the in vitro assay. While the in silico data support the pathogenicity of these two changes and both are associated with mild phenotypes, we cannot rule out these variants being non-pathogenic, and further characterization of them would be necessary.

The remaining five DPH1 variants showed a significantly greater reduction in DPH1 activity, correlating with these patients' more severe clinical presentations. The patients described by Alazami et al. [4] are homozygous for the missense variant p.(Leu234Pro), and three out of four

patients suffered an early death, with heart, renal, and CNS malformations (Table 1) and represent the most severely affected DPH1 syndrome patients. Our modeling studies suggest that this variant could shrink the entry site of the iron–sulfur cluster, and that it might decrease the distance between the cysteine residues involved in binding the iron–sulfur cluster.

The variant p.(Ala411Argfs*91) is expected to produce a longer protein and the functional studies confirm the reduction on its activity, in agreement with the severe presentation of the two siblings homozygous for this variant [8].

The variant p.(Leu164Pro) was identified in compound heterozygosity with the frameshift variant c.289delG [p.(Glu97Lysfs*8)] in two severely affected siblings [7]. The frameshift variant is located at the third exon and is predicted to be affected by the NMD process. In the *in silico* analyses, p.(Leu164Pro) variant shows an increase in the size of gate A and a slight distance increase between cysteines involved in binding of the iron–sulfur cluster.

The patients from Family 1 are homozygous for the p.(Leu125Pro) variant. Our in silico models suggest a strong effect of this change on protein structure and function. Similarly to p.(Leu234Pro), p.(Leu125Pro) decreases the distances among cysteines and reduces the entry site for the iron–sulfur cluster. Accordingly, the patients of Family 1 are among the most severely affected, including the premature death of one of them.

Finally, the patients from Family 2 are homozygous for the p.(Tyr112Cys) variant, whose activity is also clearly reduced in our assay. Residue Tyr112 is located in a central position of the entry gate of the iron–sulfur cluster, and while p.(Tyr112Cys) variant does not seem to be causing any dramatic alteration on the size of the gates, it could be affecting the iron–sulfur cluster insertion [15].

In conclusion, the four patients presented here display clinical signs compatible with the previously described patients with *DPH1* recessive variants, clearly delineating a DPH1 syndrome. We have been able to establish a good correlation between the loss of activity of various DPH1 variants in our in vitro ADPR assay, the in silico modeling, and the severity of the clinical manifestations of the patients. Thus, we demonstrate that an in vitro assay for DPH1 protein activity together with structural modeling may be useful tools for assessing DPH1 variants and predicting patients' outcomes and prognoses.

Materials and methods

All protocols were approved by the Ethics Committee of the Universitat de Barcelona (IRB00003099) (Family 1) or the Icahn School of Medicine at Mount Sinai (Family 2), and all methods were performed in accordance with the relevant guidelines and regulations. Informed consent was obtained from the patients' parents.

Whole-exome sequencing and molecular analyses

For Family 1, genomic DNA was obtained from the parents' peripheral blood and the patients' fibroblasts. Whole-exome sequencing of both patients and their parents were performed in the National Centre of Genomic Analysis (CNAG; Barcelona, Spain) using the Illumina HiSeq-2000 platform. Exome capture was performed with Agilent SureSelect v5 (Agilent, CA, USA). The filtering criteria were as in Urreizti et al. [20]. Sequencing data are available on demand.

The mean coverage was 156.84, 151.36, 217.18, and 143.30 reads for patient 1, patient 2, father, and mother, respectively, and a minimum of 99.2% of the target region was covered with at least 10 reads (C10). Six variants were selected for validation by Sanger sequencing (Supplementary Table 2). Primer sequences and PCR conditions are available on request. PCR reaction, purification, and sequencing were performed as described previously [20].

For Family 2, genomic DNA was obtained from peripheral blood. Whole-exome sequencing was performed on the proband (Patient 3) and the proband's father at Genewiz (South Plainfield, NJ, USA). An Agilent SureSelect Exome kit (v6) was used for library preparation, and sequencing was performed on an Illumina HiSeq 2500 instrument (Illumina, San Diego, CA, USA) with 100-bp, paired-end reads. Alignment and variant calling was completed with an in-house GATK-based pipeline. A total of 122,433,475 reads were generated for the proband's sample and 117,272,439 reads were generated for the father's sample. 93.2% and 94.3% of the target had ≥ 30 x coverage for the proband's and father's samples, respectively. Variants were filtered with Ingenuity Variant Analysis (Qiagen, Redwood City) based on confidence (call quality ≥ 20), frequency (variants excluded if frequency was at least 0.5% in the 1000 Genomes Project, NHLBI ESP exomes, ExAC, or gnomAD databases), predicted deleteriousness (frameshift, in-frame indel, or start/stop codon change, missense change, splice site loss up to six bases into intron or as predicted by MaxEntScan, CADD score > 15, disease-associated variant according to computed ACMG guidelines classification criteria of pathogenic or likely pathogenic, or listed in HGMD or ClinVar included). The identified *DPH1* variant was confirmed by PCR and Sanger sequencing.

Determination of DPH1 functionality

DPH1ko cells are MCF7 derivatives that have all chromosomal *DPH1* gene copies inactivated [11]. The cells lack

DPH1 enzyme activity, are diphthamide-deficient, and are resistant to diphtheria toxin. For recombinant expression of DPH1 protein and variants, DPH1ko cells were grown in RPMI/10% FCS at 37 °C in humidified 5% CO_2 and transfected with plasmids containing expression cassettes for CMV-promoter-driven transient DPH1 expression. RIPA extracts (on ice with protease inhibitor addition) were prepared 24 h thereafter. ADP-ribosylation (ADPR) of diphthamide eEF2 was evaluated in RIPA extracts of transfected DPH1ko cells as previously described [10]. Western blots of extracts + /− BioNAD–DT blocked in 5% BSA were incubated with anti-ß-actin (mouse monoclonal Ab AC-74, Sigma, cat. no. A2228 1:1500) followed by washing and incubation with anti-mouse goat polyclonal (HRP Dako, cat. no. P0447 1:1500). After additional washing and blocking in 5% BSA, streptavidin–POD was added for 1 h, the blot was washed again and developed with the HRP substrate.

Bioinformatic analyses

DPH1 protein sequences from different species were identified by BLAST using the human DPH1 protein sequence (Q9BZG8) as a query. The selected 85 protein sequences were aligned with Clustal Omega (1.2.4 version). The selection of proteins includes: 40 mammals, 9 birds, 4 reptilia, 1 amphibian (Xenopus), 7 fishes, 8 insects, 1 nematoda and 1 ascidia, 10 fungi, and 4 plants. Details of the selected proteins can be found in Supplementary Figure 2.

Homology models of variants and molecular dynamics simulations

Homology models of human DPH1–DPH2 heterodimers, with wild-type DPH2 and wild-type, p.(Tyr112Cys), p.(Leu125Pro), p.(Leu164Pro), p.(Pro221Ser), p.(Leu234-Pro), or p.(Pro382Ser) mutants of DPH1 were built using SWISSMODEL [21] using *Pyrococcus horikoshii* DPH2 homodimer structure (PDB ID: 3LZD) as a template. Human DPH1 protein was modeled from residues Glu61 to Ser389. Quality of the models was assessed with Procheck [22], with > 99% residues in allowed areas, and none of the mutated residues in disallowed regions of Ramachandran plot. In order to analyze the geometry of complex, one molecular dynamics simulation of at least 12 ns for each of our models and of the homodimeric *Pyrococcus horikoshii* DPH2–DPH2 template in water was run with Gromacs [23] using OPLS-AA force field [24]. Plots of root mean-squared deviation of the backbone versus time were used to select a time, after the initial equilibration, were backbone movements were bounded and reliable measures could be made.

Several measures were performed in these areas of the simulations: distance between S atoms of Cys115, Cys116, Cys219, and Cys347; number of hydrogen bonds between residues of DPH1 and DPH2; distances between side chain O atom of Tyr112 and CZ atom of Phe329 or NE1 of Trp354; N atom of Tyr112 and OE2 of Glu327; backbone O of Tyr112 and CE1 of His135; CD2 of His135 and CD of Gln185; CD of Gln185 and NE2 of His240, and NE2 of His240 and NE of Arg349.

Acknowledgements The authors thank the families for their participation in our research studies. We are also grateful to M. Cozar for technical assistance, and to CNAG for exome sequencing. Funding was from Associació Síndrome Opitz C, Terrassa, Spain; Spanish Ministerio de Economía y Competitividad (SAF2016-75948-R, FECYT, crowdfunding PRECIPITA), Catalan Government (2014SGR932) and from CIBERER (U720), the Mindich Child Health and Development Institute (MCHDI) at the Icahn School of Medicine at Mount Sinai, and the Genetic Disease Foundation (New York, NY).

Compliance with ethical standards

Conflict of interest RU, GDE, ES, LCV, BDG, DG, BDW, and SB declare no conflict of interest. KM and UB are employees of Roche. Roche is interested in identifying novel targets and approaches for disease diagnosis and therapy. NC is an employee of Sema4, a for-profit genetic testing laboratory. GP is employed by Lead Molecular Design, SL, a company that develops software and offers modeling services for pharmaceutical industries, but has no competing interests on the results of this article.

References

1. Collier RJ. Understanding the mode of action of diphtheria toxin: a perspective on progress during the 20th century. Toxicon. 2001;39:1793–803.
2. Chen CM, Behringer RR. Ovca1 regulates cell proliferation, embryonic development, and tumorigenesis. Genes Dev. 2004;18:320–32.
3. Yu YR, You LR, Yan YT, Chen CM. Role of OVCA1/DPH1 in craniofacial abnormalities of Miller-Dieker syndrome. Hum Mol Genet. 2014;23:5579–96.
4. Alazami AM, Patel N, Shamseldin HE, Anazi S, Al-Dosari MS, Alzahrani F, et al. Accelerating novel candidate gene discovery in neurogenetic disorders via whole-exome sequencing of prescreened multiplex consanguineous families. Cell Rep. 2015;10:148–61.
5. Loucks CM, Parboosingh JS, Shaheen R, Bernier FP, McLeod DR, Seidahmed MZ, et al. Matching two independent cohorts validates DPH1 as a gene responsible for autosomal recessive intellectual disability with short stature, craniofacial, and ectodermal anomalies. Hum Mutat. 2015;36:1015–9.
6. Riazuddin S, Hussain M, Razzaq A, Iqbal Z, Shahzad M, Polla DL, et al. Exome sequencing of Pakistani consanguineous families identifies 30 novel candidate genes for recessive intellectual disability. Mol Psychiatry. 2017;22:1604–14.
7. Nakajima J, Oana S, Sakaguchi T, Nakashima M, Numabe H, Kawashima H, et al. Novel compound heterozygous DPH1

mutations in a patient with the unique clinical features of airway obstruction and external genital abnormalities. J Hum Genet. 2018;63:529–32.
8. Sekiguchi F, Nasiri J, Sedghi M, Salehi M, Hosseinzadeh M, Okamoto N, et al. A novel homozygous DPH1 mutation causes intellectual disability and unique craniofacial features. J Hum Genet. 2018;63:487–91.
9. Stahl S, Mueller F, Pastan I, Brinkmann U. Factors that determine sensitivity and resistances of tumor cells towards antibody-targeted protein toxins. In: Verma R, Bonavida B, (eds.). Resistance to Immunotoxins in Cancer Therapy. Resistance to Targeted Anti-Cancer Therapeutics 6. Cham: Springer; 2015. p. 57–73.
10. Mayer K, Schroder A, Schnitger J, Stahl S, Brinkmann U. Influence of DPH1 and DPH5 protein variants on the synthesis of Diphthamide, the target of ADPRibosylating toxins. Toxins. 2017;9:78.
11. Stahl S, da Silva Mateus Seidl AR, Ducret A, Kux van Geijtenbeek S, Michel S, Racek T, et al. Loss of diphthamide pre-activates NF-kappaB and death receptor pathways and renders MCF7 cells hypersensitive to tumor necrosis factor. Proc Natl Acad Sci USA. 2015;112:10732–7.
12. Zhang Y, Zhu X, Torelli AT, Lee M, Dzikovski B, Koralewski RM, et al. Diphthamide biosynthesis requires an organic radical generated by an iron-sulphur enzyme. Nature. 2010;465:891–6.
13. Broderick JB, Duffus BR, Duschene KS, Shepard EM. Radical S-adenosylmethionine enzymes. Chem Rev. 2014;114:4229–317.
14. Liu S, Milne GT, Kuremsky JG, Fink GR, Leppla SH. Identification of the proteins required for biosynthesis of diphthamide, the target of bacterial ADP-ribosylating toxins on translation elongation factor 2. Mol Cell Biol. 2004;24:9487–97.
15. Maio N, Rouault TA. Iron-sulfur cluster biogenesis in mammalian cells: new insights into the molecular mechanisms of cluster delivery. Biochim Biophys Acta. 2015;1853:1493–512.
16. Dong M, Kathiresan V, Fenwick MK, Torelli AT, Zhang Y, Caranto JD, et al. Organometallic and radical intermediates reveal mechanism of diphthamide biosynthesis. Science. 2018;359:1247–50.
17. Uniprot Consortium, T. UniProt: the universal protein knowledgebase. Nucleic Acids Res. 2017;45:D158–D169.
18. Salamov AA, Nishikawa T, Swindells MB. Assessing protein coding region integrity in cDNA sequencing projects. Bioinformatics. 1998;14:384–90.
19. Wernersson R. Virtual Ribosome--a comprehensive DNA translation tool with support for integration of sequence feature annotation. Nucleic Acids Res. 2006;34:W385–8.
20. Urreizti R, Cueto-Gonzalez AM, Franco-Valls H, Mort-Farre S, Roca-Ayats N, Ponomarenko J, et al. A De novo nonsense mutation in MAGEL2 in a patient initially diagnosed as Opitz-C: similarities between Schaaf-Yang and Opitz-C syndromes. Sci Rep. 2017;7:44138.
21. Biasini M, Bienert S, Waterhouse A, Arnold K, Studer G, Schmidt T, et al. SWISS-MODEL: modelling protein tertiary and quaternary structure using evolutionary information. Nucleic Acids Res. 2014;42:W252–8.
22. Morris AL, MacArthur MW, Hutchinson EG, Thornton JM. Stereochemical quality of protein structure coordinates. Proteins. 1992;12:345–64.
23. Abraham MJ, Murtola T, Schulz, Páll S, Smith JC, Hess B, et al. GROMACS: high performance molecular simulations through multi-level parallelism from laptops to supercomputers. SoftwareX. 2015;1-2:19–25.
24. Jorgensen WL, Maxwell DS, Tirado-Rives J. Development and testing of the OPLS all-atom force field on conformational energetics and properties of organic liquids. J Am Chem Soc. 1996;118:11225–36.